

# The Determination of Cis–Trans Conformations in Tetrahedral *p*-Phenylene Vinylene Oligomers

John E. Bushnell, Paul R. Kemper, Guillermo C. Bazan, and Michael T. Bowers\*

Department of Chemistry & Biochemistry, University of California, Santa Barbara, California 93106

Received: May 4, 2004; In Final Form: July 15, 2004

Time-of-flight mass spectrometry and ion-mobility studies were used to probe the conformations of a tetrahedral oligo *p*-phenylene vinylene sample. The radical cation and sodiated parent species as well as one fragmented ion were analyzed using ion mobility. Extensive molecular mechanics modeling was used to understand the effects that secondary structure has on the observed cross sections from ion-mobility experiments. The major features in the ion-mobility spectra appear to be due to arm–arm interactions caused by cis defects near the tetrahedral core of these oligomers.

## 1. Introduction

Conjugated organic polymers have been the object of intense research since their viability for use in optoelectronic devices was shown in the early 1990s.<sup>1–4</sup> They are extremely attractive for the production of devices such as organic light-emitting diodes (OLEDs) and field-effect transistors due to their ease of handling and tunability. Their properties can be tuned via chemical functionalization, and in some cases production can be accomplished via spray techniques as opposed to far more expensive methods used in processing traditional metal semiconductors. One of the first organic polymers that has shown promise as an organic semiconductor is poly(*p*-phenylenevinylene) (PPV), usually containing alkoxy side groups to render them soluble. More recently, smaller oligomers of phenylene vinylene have been synthesized, which has enabled research on a more fundamental level due to the more precise control over their synthesis.<sup>5–7</sup> Properties of interest include their photophysics, morphology, and resistance to degradation. Smaller oligomers offer the advantages of better purity and synthetic control compared to larger polymers.

Recently, we have used ion-mobility measurements to study the size distributions of oligo-PPVs containing five and six phenyl rings.<sup>8</sup> As opposed to the putative trans conformation of vinyl linkages, it was found that these PPV “arms” contained a significant amount of cis defects. As the ion-mobility apparatus was coupled to a mass spectrometer, it was clear that these defects were not due to saturated tetrahedral linkages as has been postulated for poly-PPV.<sup>9,10</sup> Additional results utilizing near-field single-molecule spectroscopy showed excellent agreement between the shape distribution of oligo-PPVs and their fluorescence anisotropy.<sup>8</sup> Ion mobility has also been used to determine the distribution of conformations in *p*-cyclophanes and various other polymers.<sup>11–15</sup> This technique is especially useful in sorting out different conformations for compounds of identical mass and in cases where NMR assignments are difficult or impossible.

An important property for luminescent organic materials is the ability to form stable, amorphous films.<sup>7,16</sup> While small oligo-PPV “arms” readily form crystalline structures when

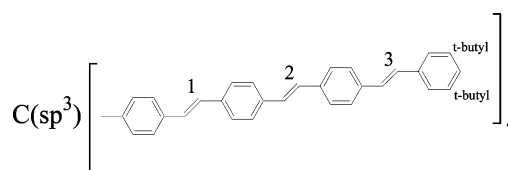


**Figure 1.** The two-dimensional representation of T4R.

deposited from solution, more exotic shapes have been sought which resist crystallization and thus exist as stable glasses.<sup>7</sup> One of these approaches is to join four PPV “arms” together in a tetrahedral arrangement about a central carbon atom.<sup>16</sup> In this paper, we use the ion-mobility technique to examine the conformations of a sample of tetrakis(4-(4′-(3′′,5′′-di-*tert*-butylstyryl)styryl)stilbenyl)methane, a tetrahedral oligo-PPV with each PPV “arm” containing four phenyl rings. This compound will be referred to as T4R for brevity and is shown in Figure 1. The “T” represents the tetrahedral arrangement of arms about the central  $\text{sp}^3$  carbon atom, and the “4R” indicates that there are four phenyl rings within each arm. A fragment observed in the mass spectrum, which corresponds to the loss of one arm from T4R, will be referred to here as P4R, where the “P” indicates the planar configuration about the central carbon.

With the help of molecular dynamics calculations, we identify the intramolecular interactions responsible for broad families of secondary structures seen in the ion-mobility spectra and assess the ion-mobility method as an analytical tool for measuring the distribution of defects in a sample containing a wide distribution of conformations.

## 2. Instrumentation

The instrument used in these studies has been described previously.<sup>17</sup> A diagram of the instrument is shown in Figure 2.

It utilizes a matrix-assisted laser desorption/ionization (MALDI) ion source. Ions produced in the MALDI source are accelerated using a two-stage Wiley–McLaren-type system into a 1 m long reflectron time-of-flight (TOF) mass spectrometer. For ion-mobility studies, the TOF sector is operated in linear mode (the reflectron is turned off). The mass peak of interest is gated at the end of the flight tube, decelerated, and injected

\* To whom correspondence may be addressed. E-mail: bowers@chem.ucsb.edu.

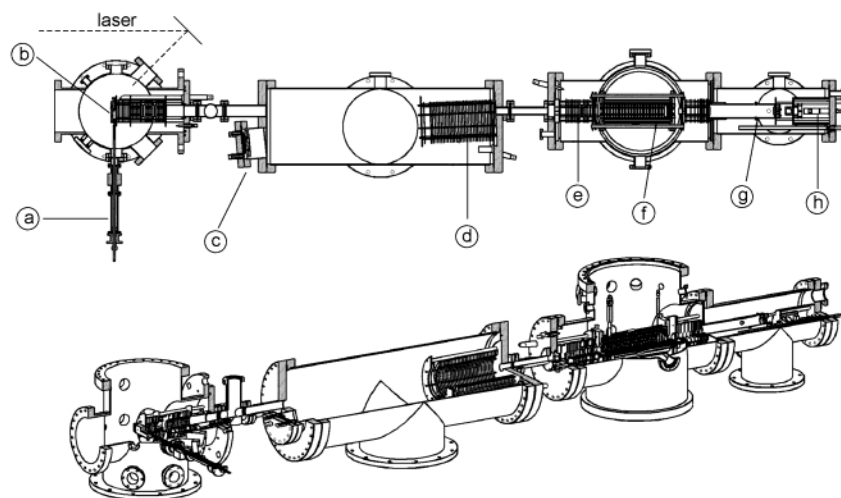


**Figure 2.** Schematic of the overall instrument used in this study: (a) sample probe; (b) sample inside the MALDI source; (c) detector used when the TOF is operated in reflectron mode; (d) reflectron; (e) deceleration lenses; (f) drift cell; (g) quadrupole; (h) detector used for the ion-mobility experiments.

into a 20 cm long drift cell containing 1.6 Torr He at 300 K. Ions are quickly thermalized by collisions with the He bath gas and pulled through the drift cell under the influence of a small electric field. Ions reaching the drift cell exit orifice are accelerated slightly into a quadrupole for mass analysis and then detected using pulse-counting techniques. Ions are collected as a function of time, with the start time triggered by the source extraction pulse.

The sample PPV compound was dissolved in THF solvent at a concentration of about 0.5 mg/mL. About 5  $\mu$ L of saturated NaI in methanol was added to 100  $\mu$ L of OPV/THF solution, and the final sample-containing solution was applied to the outside of a stainless steel rod and dried. The sample was inserted into the MALDI source, and a stepper motor rotated and translated the stainless steel rod, exposing fresh areas of sample to the laser. A nitrogen laser (Lasertechnik Berlin MSG 400,  $\lambda = 337$  nm) was used to desorb and ionize the sample. The laser is usually operated at 30 Hz and has a pulse width of <10 ns and a maximum average power of 12 mW. Note that in these experiments no matrix was necessary since PPVs undergo direct photoionization.

### 3. The Ion-Mobility Experiment

Within the drift cell, ions move through the cell under the influence of a weak applied electric field. The electric field is “weak” in the sense that the internal energy of the ions is in thermal equilibrium with the buffer gas. Diffusion of ions in this so-called low-field region has been well characterized.<sup>18</sup> Within this low-field limit, the drift velocity ( $v_D$ ) of an ion is proportional to the applied electric field ( $E$ ) as shown in eq 1. The constant of proportionality is

$$v_D = KE \quad (1)$$

known as the **mobility**,  $K$ . The mobility of an ion can be related to its collision **cross section** ( $\sigma$ ) via eq 2, where  $e$  is the ion’s charge,  $N$  is the particle density of the buffer gas,  $\mu$  is the reduced mass of the ion and buffer gas,  $k_b$  is the Boltzman

$$K = \frac{3e}{16N} \left( \frac{2\pi}{\mu k_b T} \right)^{1/2} \frac{1}{\sigma} \quad (2)$$

constant, and  $T$  is the temperature.<sup>18</sup> Thus the mobility of an ion and its collision cross section are inversely proportional.

This means that a more compact structure, having a smaller cross section, will have a higher mobility and thus move more quickly through the drift cell. Therefore, the ion-mobility experiment is able to separate ions based on their relative sizes, with smaller ions arriving at earlier times and larger ions arriving at later times. Specifically, ion-mobility experiments are able to distinguish ions of the same mass based on their size in cases where different isomers have significantly different collisional cross sections.

By use of structural models (see below), it is possible to estimate the cross sections,  $\sigma$ , for various isomers or configurations and compare these with experiment in order to gain some structural information based on an ion’s observed mobility. In cases where multiple structures are not fully resolved, it is possible to model arrival time distributions (ATD) by adding together components having different cross sections. In this way, the relative amounts of various components can be determined by fitting the modeled spectrum to the experimental spectrum.

### 4. Structural Modeling

To model the structures of PPV ions, the Amber molecular mechanics force field was used.<sup>19</sup> This force field has given very good agreement with experiment in previous ion-mobility studies<sup>11–15</sup> and more sophisticated ab initio methods are prohibitively expensive for systems of this size. Most of the parameters necessary were available in the Amber “1999” force field, and missing parameters were chosen by analogy from already defined parameters. The center carbon in P4R<sup>+</sup> was treated as a trigonal planar,  $sp^2$  center. All vinyl linkages were explicitly modeled as cis or trans, with custom atom types used for the  $sp^2$  carbons involved in these bonds. This allowed the use of single-fold dihedral potentials which prevented inter-conversion of cis and trans species during simulated annealing. See the Supporting Information for a discussion of parameters used in the Amber calculations. Charges were determined using DFT (B3LYP/6-31G\*) optimized model substructures and subsequent processing of Mulliken charges using the RESP method of Amber. Charges were determined for subunits which were used to build the full molecules using Amber’s leap interface. See the Supporting Information for a listing of the derived charges.

After building a full set of parameters and atomic charges needed in Amber, simulated annealing was carried out on a large

set of possible cis/trans isomers. For each isomer that was calculated, the newly built structure was first geometry minimized. Then molecular dynamics was run for 30 ps at high temperature (600–800 K), the nascent “hot” molecule stepwise cooled over a 10 ps period, and the final structure again fully minimized. This annealing cycle was repeated 300 times for each isomer, creating an energy profile of minimized candidate structures. Finally, the cross sections of the five lowest energy structures were averaged to give the final theoretical cross section for that isomer. Cross sections were calculated using a straightforward projection approximation<sup>20,21</sup> that has compared very favorably with experiment for molecules in the size range studied here.<sup>12,13,15,22,23</sup>

In the case of T4R–Na<sup>+</sup>, structures and cross sections were calculated for all isomers containing up to three cis defects. These results closely mirrored the results for T4R<sup>+</sup>, so no further modeling of T4R–Na<sup>+</sup> was done, and cross sections for T4R<sup>+</sup> were used to model the ATD of T4R–Na<sup>+</sup> (see below).

### 5. Modeling Arrival Time Distributions

To compare calculated cross sections for a group of cis/trans isomers with the experimentally observed arrival time distribution, ATDs for each individual isomer were calculated by taking into account the physical dimensions of the drift cell and the experimental conditions. These in turn were combined to form a weighted average to directly compare with the experimental ATD. The functional form of the component ATDs used is shown in eq 3, where  $I(t)$  is the signal intensity exiting the drift

$$I(t) = \frac{1}{(4\pi D_L t)^{1/2}} \left[ 1 - \exp\left(-\frac{r_0^2}{4D_T t}\right) \right] \exp\left(-\frac{(z - v_D t)^2}{4D_L t}\right) \quad (3)$$

cell,  $D_L$  is the longitudinal diffusion coefficient,  $t$  is the time,  $r_0$  is the exit orifice radius,  $D_T$  is the transverse diffusion coefficient,  $z$  is the drift cell length, and  $v_D$  is the drift velocity.<sup>18</sup> The longitudinal and transverse diffusion coefficients are estimated based on the polarization model using eq 4, where  $M$  is the mass of the buffer gas,  $m$  is the mass of the ion  $e$  is the

$$D_L = D(0) + \frac{(M + 3.72m)M}{3(M + 1.908m)e} \frac{v_D^3}{E} \quad (4)$$

charge on the ion,  $v_D$  is again the drift velocity,  $E$  is the applied electric field, and  $D(0)$  is the diffusion coefficient calculated using the Einstein equation, shown in eq 5, where  $K$  is the ion's

$$K = \frac{eD}{kT} \quad (5)$$

mobility,  $e$  is the charge,  $k$  is the Boltzmann constant, and  $T$  is the temperature (see ref 18 for details).

For the systems in this study, a large number of cis/trans isomers are possible due to the number of vinyl linkages present. T4R<sup>+</sup> contains 12 vinyl linkages leading to  $2^{12} = 4096$  possible isomers. However, as optical isomers have identical cross sections and the various arms are indistinguishable, there are only 330 unique isomers for T4R<sup>+</sup>. In the case of P4R<sup>+</sup>, there are 120 unique isomers. Fitting spectra using such a large set of components would give little useful information. However, the number of parameters can be vastly reduced by making two simplifying assumptions: (1) The probability of each vinyl linkage is completely independent of the other vinyl groups and (2) the probability of being cis or trans for each vinyl linkage is determined by the position of the vinyl group along the arm.

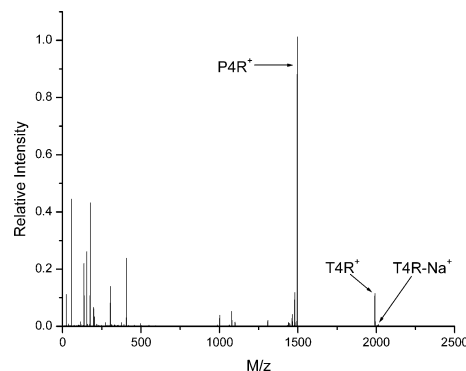


**Figure 3.** The TOF mass spectrum obtained in reflectron mode.

Thus we can define three probabilities,  $P_{\text{cis}}(1)$ ,  $P_{\text{cis}}(2)$ , and  $P_{\text{cis}}(3)$ , which are the probabilities of a vinyl linkage being cis in positions 1, 2, and 3, respectively (see Figure 1). The probability for each unique isomer can then be assembled using these three probabilities plus a degeneracy factor corresponding to the number of isomers that correspond to each particular (unique) isomer. This degeneracy factor simply maps the set of 330 unique isomers to the full set of 4096 possible isomers (in the case of T4R<sup>+</sup>). A straightforward Fortran program was written which calculates each component's ATD using eq 3, above, and sums them together using  $P_{\text{cis}}(1)$ ,  $P_{\text{cis}}(2)$ , and  $P_{\text{cis}}(3)$  as described above. In this way, the experimental ATDs were fit using only these three parameters.

### 6. Results and Discussion

The MALDI/TOF mass spectrum of the T4R PPV sample is shown in Figure 3.

The largest peak in the spectrum has a mass-to-charge ratio of 1497 Da and corresponds to the parent ion after the loss of one “arm”. That is, the center carbon is only bonded to three carbons, leading to an  $sp^2$ , trigonal planar type structure. We refer to this species as P4R<sup>+</sup> in this paper to denote “Planar” as opposed to “Tetrahedral”. At higher mass, the T4R<sup>+</sup> parent ion is seen as well as the sodiated parent. Note that the parent ion appears at 1992 Da, corresponding to the radical cation rather than a protonated species. A small peak at 1002 Da corresponds to the loss of two arms from the T4R parent, and the lower mass peaks are mostly attributable to DHB matrix peaks as well as Na<sup>+</sup> and a C<sub>4</sub>H<sub>9</sub><sup>+</sup> fragment. The large peak corresponding to the loss of one arm from T4R is somewhat surprising, and it is unclear whether this peak is the result of an impurity in the sample or is due to an unexpectedly strong dissociation mechanism leading to cleavage of one of the central C–C bonds.

ATDs were recorded for the parent T4R<sup>+</sup>, sodiated T4R–Na<sup>+</sup>, and P4R<sup>+</sup> species and are shown in Figure 4.

The ATDs for T4R<sup>+</sup> and T4R–Na<sup>+</sup> are similar with a small shoulder at the longest times, and two very broad features at shorter times. The ATD for P4R<sup>+</sup> is quite different, with two broad features at longer times, and a broad shoulder containing a distinct peak at shorter time. The signal-to-noise in the ATD for P4R<sup>+</sup> is significantly better than the parent ion and sodiated species due to the much higher intensity seen for that species in the mass spectrum. Note that the very large differences in arrival times of at least 50% in these ATDs indicate a size difference on the order of 65% between the largest and smallest conformations. The width of an ATD peak composed of a single conformation of this size would be on the order of only 0.1 ms.

As described in section 4, simulated annealing was performed using the Amber force field/software suite<sup>19</sup> to get information

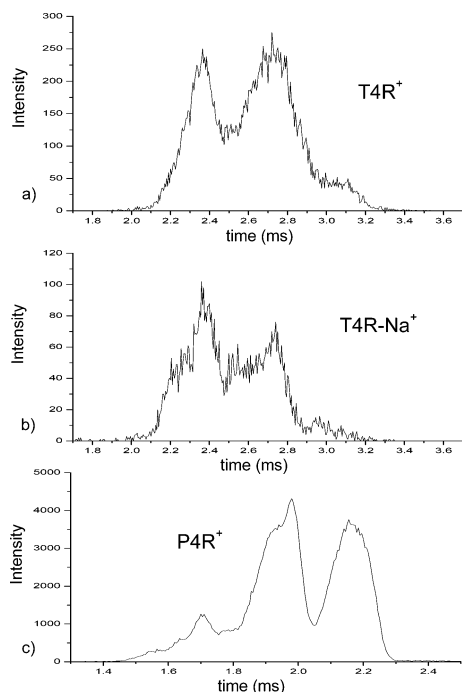


**Figure 4.** ATDs in 1.6 Torr of He at 300 K: (a)  $T4R^+$ ; (b)  $T4R-Na^+$ ; (c)  $P4R^+$ .

about the various conformations represented in the ATDs. Representative structures for the all-trans structures (that is, containing no cis defects) are shown in Figure 5.  $T4R^+$  has a pseudo tetrahedral structure while  $P4R^+$  is pseudo trigonal planar. The structure of  $T4R-Na^+$  is essentially identical to  $T4R^+$ , with the  $Na^+$  lying midway between the innermost phenyl rings of two arms in the lower energy calculated structures.

The large set of structures calculated for  $T4R^+$  and  $P4R^+$  were used to model ATDs as described in section 5. Each of the ATDs were modeled using only the three parameters  $P_{cis}(1)$ ,  $P_{cis}(2)$ , and  $P_{cis}(3)$ . The resulting fits along with the experimental spectra for comparison are shown in Figure 6 along with the fit parameters (cis probabilities) in Table 1.

Uncertainties are estimated to be on the order of  $\pm 0.05$  (5%). The agreement between modeled and experimental ATDs is remarkable considering that only three parameters were used to determine the populations of hundreds of isomers. The reduction of probabilities to only three parameters completely ignores nearest-neighbor effects of chemical or steric origin as well as any interactions between different arms. The probabilities for cis defects are mostly similar between the different species, giving an average probability of 0.29 for any given vinyl group having a cis conformation.

While the overall probability of cis defects is a useful quantity to measure, molecular modeling gives a richer understanding of the secondary structure in these ions. Figure 7 shows the modeled ATD for  $T4R^+$  along with individual components for comparison (scaled to an arbitrary intensity for visibility).

The peak labeled trans contains no cis defects, while the peak labeled cis has all of its vinyl linkages in the cis conformation. C1, C1C1, etc. refer to a single cis defect in the first ("1") position, two cis defects both in the first position, etc. Clearly, the set of isomers from no cis defects to all cis defects nicely spans the experimental spectrum. The origin of the broad features can be understood by looking at the C1 structures shown in Figure 8.

The presence of a single C1 defect allows a single arm–arm interaction, a partial folding, that significantly reduces the cross

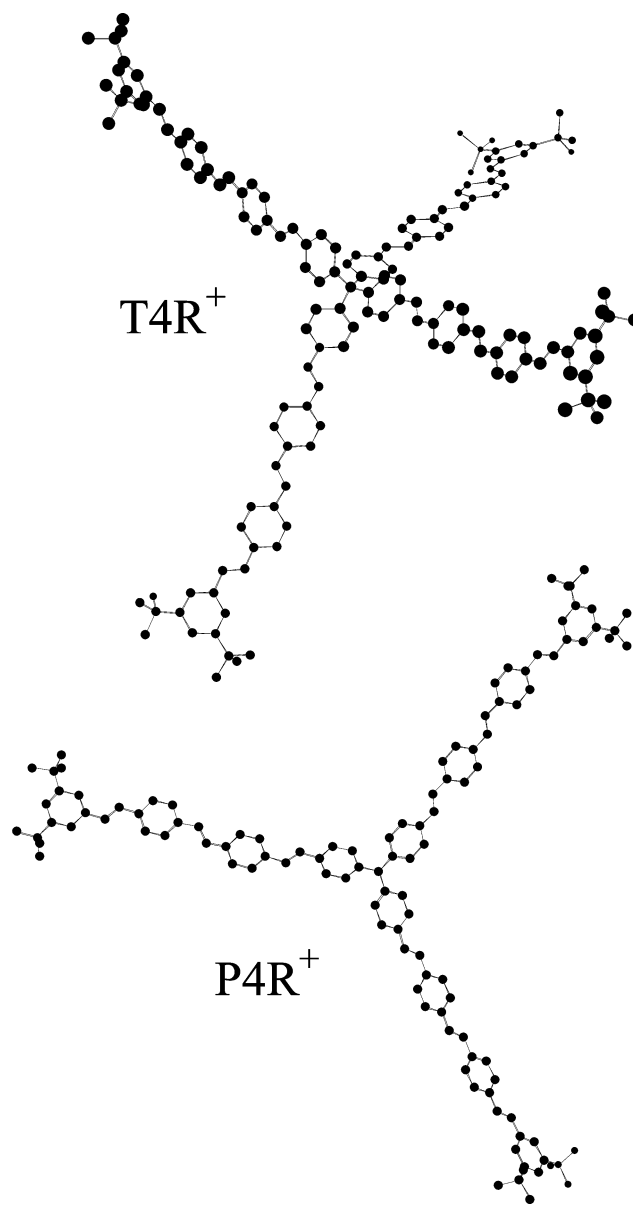


**Figure 5.** Representative structures from molecular mechanics of  $T4R^+$  (top) and  $P4R^+$  (bottom).

section. A single C2 or C3 defect is insufficient to cause two arms to fold together according to the molecular modeling. The second C1 defect leads to a second arm–arm interaction and roughly corresponds to the beginning of the second broad feature (working from right to left). The third and fourth C1 defects lead to additional folding, all lying within the second broad feature. The results of fitting the modeled spectrum to experiment includes similar amounts of C2 and C3 defects, and these additional defects account for the filling out of the peaks toward the left (smaller cross sections thus shorter arrival times).

The same qualitative analysis can be applied to  $P4R^+$ . The modeled ATD for  $P4R^+$  and some selected components are shown in Figure 9.

Here we clearly see a difference in folding thresholds. As can be seen in Figure 10, the first C1 defect leads to an arm–arm folding interaction as in  $T4R^+$ .

However, the second C1 defect is predicted to give a similar structure. It is not until the third C1 defect that all three arms fold together. This, along with the different statistics of this three-armed system, leads to a markedly different ATD for  $P4R^+$  compared with  $T4R^+$ .



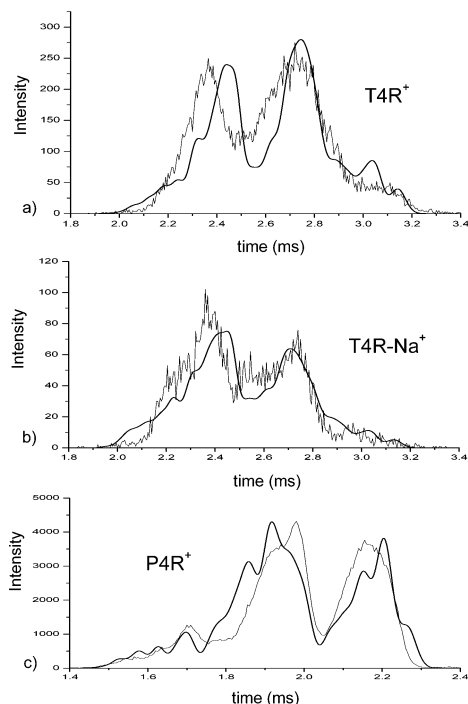


**Figure 6.** Calculated ATDs shown with experimental ATDs for comparison: (a) T4R<sup>+</sup>; (b) T4R-Na<sup>+</sup>; (c) P4R<sup>+</sup>.

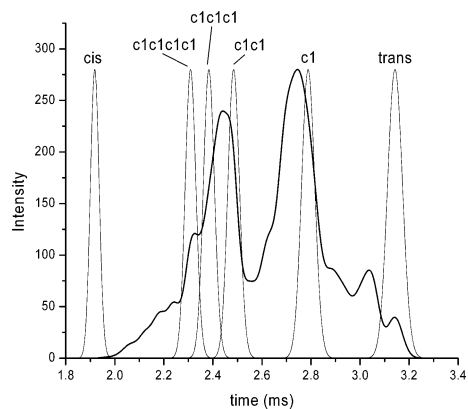


**Figure 7.** The modeled ATD for T4R<sup>+</sup> showing representative components.

**TABLE 1: Cis Probabilities from ATD Fits**

ion	P <sub>cis</sub> (1)	P <sub>cis</sub> (2)	P <sub>cis</sub> (3)
T4R <sup>+</sup>	.3	.2	.3
T4R-Na <sup>+</sup>	.35	.3	.3
P4R <sup>+</sup>	.16	.36	.3

The smaller feature to the left in Figure 4C, at an arrival time of about 1.7 ms, corresponds nicely with the structure of C1C1C2 from the modeling (see Figures 6C and 9). While the structure of C1C1 is almost the same size as C1, an additional C2 defect gives a structure for P4R<sup>+</sup> nearly as compact as C1C1C1 (see Figure 9).

## 7. Conclusions

We have shown that it is possible to obtain quantitative information on the amount and location of cis defects within a complex mixture of OPVs. This was only possible due to the application of extensive molecular modeling to possible isomers and making some simplifying (though not grossly unreasonable) assumptions about the statistics of cis defects.

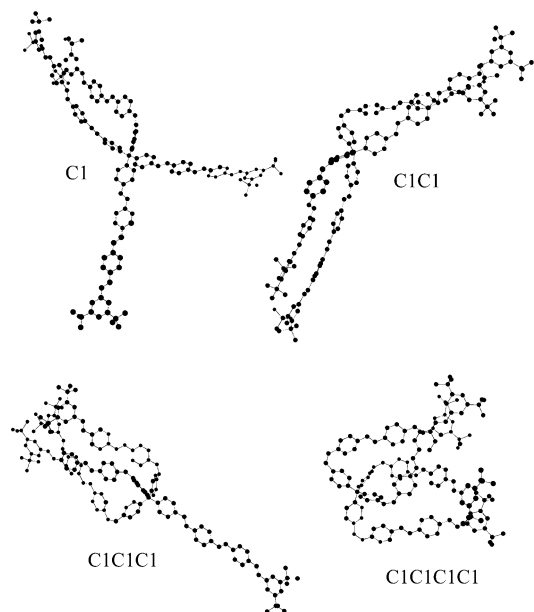


**Figure 8.** Representative structures of T4R<sup>+</sup> containing cis (1) defects from molecular mechanics.

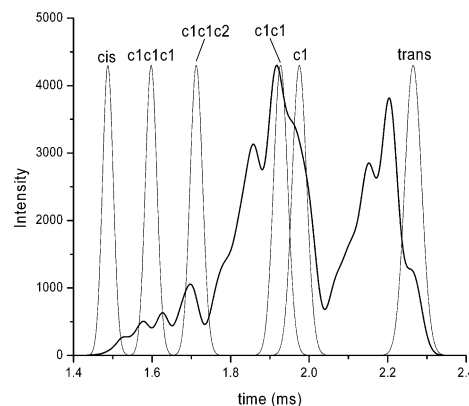


**Figure 9.** The modeled ATD for P4R<sup>+</sup> showing representative components.

We note that there are several reasons why we believe that the structures of these compounds do not change upon ionization and directly reflect the structures in the solid neutral sample. The wavelength of the desorbing laser is such that resonant 2-photon ionization should be the primary source of ions, leaving the newly formed ions in a relatively cold state,<sup>24</sup> while the barrier to cis/trans isomerization is estimated to be about 50 kcal/mol.<sup>25</sup> Identical experiments performed on pure samples of cis and trans stilbene gave exclusively the cis or trans parent, respectively, indicating that cis/trans rearrangement does not occur. And in a recent study of much simpler PPV “arms”, individual defect structures were highly resolvable and were well correlated with single-molecule photophysics of the neutrals.<sup>8</sup>

While this study involved extensive molecular modeling, this technique is a useful tool for rapid analysis and feedback to synthetic chemists. Once the initial modeling has been completed, it is trivial to analyze subsequent ATDs using the same set of calculated cross sections. Approximately 25 μg are typically needed for a single analysis, and spectra can be acquired in a few minutes, with far greater detail than afforded by size exclusion chromatography. And mass selection makes the identity of analyte unambiguous.

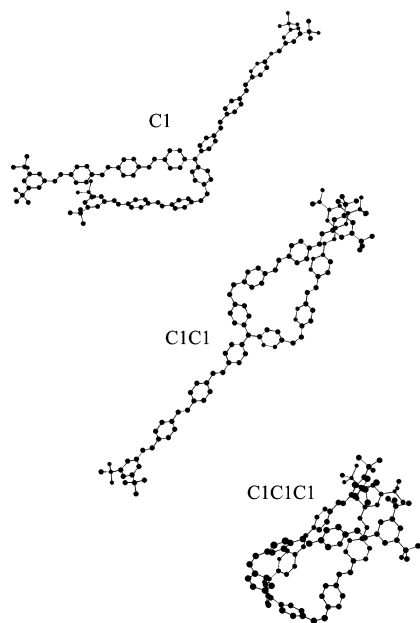


**Figure 10.** Representative structures of P4R<sup>+</sup> containing cis (1) defects from molecular mechanics.

**Acknowledgment.** The support of the Air Force Office of Scientific Research under Grant No. F49620-03-1-0046 is gratefully acknowledged.

**Supporting Information Available:** A description and listing of custom Amber force field parameters and charges used in the molecular dynamics studies. This material is available free of charge via the Internet at <http://pubs.acs.org>.

## References and Notes

- (1) Burroughes, J. H.; Bradley, D. D. C.; Brown, A. R.; Marks, R. N.; Mackay, K.; Friend, R. H.; Burns, P. L.; Holmes, A. B. *Nature* **1990**, *347*, 539.
- (2) Braun, D.; Heeger, A. J. *Appl. Phys. Lett.* **1991**, *58*, 1982.
- (3) Gustafsson, G.; Cao, Y.; Treacy, G. M.; Klavetter, F.; Colaneri, N.; Heeger, A. J. *Nature* **1992**, *357*, 477.

- (4) Grem, G.; Leditzky, G.; Ullrich, B.; Leising, G. *Adv. Mater.* **1992**, *4*, 36.
- (5) Robinson, M. R.; Wang, S.; Bazan, G. C.; Cao, Y. *Adv. Mater.* **2000**, *12*, 1701.
- (6) Oldham, W. J., Jr.; Lachicotte, R. J.; Bazan, G. C. *J. Am. Chem. Soc.* **1998**, *120*, 2987.
- (7) Robinson, M. R.; Wang, S.; Heeger, A. J.; Bazan, G. C. *Adv. Funct. Mater.* **2001**, *11*, 413.
- (8) Summers, M. A.; Kemper, P. R.; Bushnell, J. E.; Robinson, M. R.; Bazan, G. C.; Bowers, M. T.; Buratto, S. K. *J. Am. Chem. Soc.* **2003**, *125*, 5199.
- (9) Hu, D.; Yu, J.; Wong, K.; Bagchi, B.; Rossky, P. J.; Barbara, P. F. *Nature* **2000**, *405*, 1030.
- (10) Wong, K. F.; Skaf, M. S.; Yang, C.-Y.; Rossky, P. J.; Bagchi, B.; Hu, D.; Yu, J.; Barbara, P. F. *J. Phys. Chem. B* **2001**, *105*, 6103.
- (11) Baker, E. S.; Hong, J. W.; Gidden, J.; Bartholomew, G. P.; Bazan, G. C.; Bowers, M. T. *J. Am. Chem. Soc.* **2004**, *126*, 6255.
- (12) Gidden, J.; Bowers, M. T.; Jackson, A. T.; Scrivens, J. H. *J. Am. Soc. Mass Spec.* **2002**, *13*, 499.
- (13) Gidden, J.; Wyttenbach, T.; Jackson, A. T.; Scrivens, J. H.; Bowers, M. T. *J. Am. Chem. Soc.* **2000**, *122*, 4692.
- (14) Gidden, J.; Wyttenbach, T.; Batka, J. J.; Weis, P.; Bowers, M. T.; Jackson, A. T.; Scrivens, J. H. *J. Am. Soc. Mass Spectrom.* **1999**, *10*, 883.
- (15) Gidden, J.; Jackson, A. T.; Scrivens, J. H.; Bowers, M. T. *Int. J. Mass Spectrom.* **1999**, *188*, 121.
- (16) Wang, S.; Oldham, W. J., Jr.; Hudack, R. A., Jr.; Bazan, G. C. *J. Am. Chem. Soc.* **2000**, *122*, 5695.
- (17) Baker, E. S.; Gidden, J.; Fee, D. P.; Kemper, P. R.; Anderson, S. E.; Bowers, M. T. *Int. J. Mass Spectrom.* **2003**, *227*, 205.
- (18) McDaniel, E. W.; Mason, E. A. *The Mobility and Diffusion of Ions in Gases*; Wiley: New York, 1973.
- (19) Case, D. A.; Pearlman, D. A.; Caldwell, J. W.; Cheatham, T. E., III.; Wang, J.; Ross, W. S.; Simmerling, C. L.; Darden, T. A.; Merz, K. M.; Stanton, R. V.; Cheng, A. L.; Vincent, J. J.; Crowley, M.; Tsui, V.; Gohlke, H.; Radmer, R. J.; Duan, Y.; Pitera, J.; Massova, I.; Seibel, G. L.; Singh, U. C.; Weiner, P. K.; Kollman, P. A. *AMBER 7*; University of California: San Francisco, 2002.
- (20) von Helden, G.; Wyttenbach, T.; Bowers, M. T. *Int. J. Mass Spectrom. Ion Processes* **1995**, *146/147*, 349.
- (21) Wyttenbach, T.; von Helden, G.; Batka, J. J., Jr.; Carlat, D.; Bowers, M. T. *J. Am. Soc. Mass Spectrom.* **1997**, *8*, 275.
- (22) Gidden, J.; Wyttenbach, T.; Batka, J. J.; Weis, P.; Jackson, A. T.; Scrivens, J. H.; Bowers, M. T. *J. Am. Chem. Soc.* **1999**, *121*, 1421.
- (23) Wyttenbach, T.; von Helden, G.; Bowers, M. T. *Int. J. Mass Spectrom. Ion Processes* **1997**, *165/166*, 377.
- (24) Pedley, J. B.; Rylance, J. Sussex NPL. Computer Analyzed Thermochemical Data: Organic and Organometallic Compounds, University of Sussex, U.K.; 1977.
- (25) Soltiel, J.; Garapathy, S.; Werking, C. *J. Phys. Chem.* **1987**, *91*, 2755.